Monthly Notices
of the
ROYAL ASTRONOMICAL SOCIETY

MNRAS **490,** 5647–5657 (2019) doi:10.1093/mnras/stz2959

Searching for correlations in *Gaia* DR2 unbound star trajectories

F. Montanari [1]★ D. Barrado [2]★ and J. García-Bellido [1]★

[1] *Instituto de Física Teórica IFT–UAM/CSIC, Universidad Autónoma de Madrid, Cantoblanco, 28049 Madrid, Spain*
[2] *Departamento de Astrofísica, Centro de Astrobiología (CSIC–INTA), ESA–ESAC, Camino Bajo del Castillo s/n, 28692 Villanueva de la Cañada, Madrid, Spain*

Accepted 2019 October 18. Received 2019 October 16; in original form 2019 July 23

ABSTRACT

Scattering events with compact objects are expected in the primordial black hole (PBH) cold dark matter (CDM) scenario, due to close encounters between stars and PBHs in the dense environments of dwarf spheroidals. We develop a Bayesian framework to search for correlations among Milky Way stellar trajectories and those of globular clusters and dwarf galaxies in the halo and in other nearby galaxies. We apply the method to a selection of hypervelocity stars (HVS) and globular clusters from the *Gaia* DR2 catalogue and known nearby (mostly dwarf) galaxies with full phase-space and size measurements. We report positive evidence for trajectory intersection ∼20–40 Myr ago of up to two stars, depending on priors, with the Sagittarius dwarf spheroidal galaxy (dSph) when assuming the distance estimates of Marchetti, Rossi & Brown (2018). We verify that the result is compatible with their evolutionary status, setting a lower bound for their stellar age of ∼100 Myr. However, such scattering events are not confirmed when assuming Anders et al. (2019) distance estimates. We discuss shortcomings related to present data quality and future prospects for detection of HVS with the full *Gaia* catalogue and Sagittarius dSph.

Key words: Galaxy: kinematics and dynamics – Galaxy: stellar content – galaxies: kinematics and dynamics – galaxies: statistics – dark matter.

1 INTRODUCTION

The hierarchical structure formation scenario assumes that large galaxies are formed by mergers of smaller ones, which bring in gas (hydrogen), stars and dark matter (DM). These smaller structures, generically called dwarf galaxies, orbit around the larger galaxy and interact with it. Some appear tidally disrupted by previous crossings through the disc and are elongated, and others are still approaching it and have a more-or-less spherical shape. All such substructures have large mass-to-light ratios, in some cases larger than 1000, making them extremely difficult to detect in the sky. Their numbers were predicted, within the cold dark matter scenario, to be large, hundreds to thousands of objects orbiting each large galaxy. However, only about a dozen had been observed until the Sloan Digital Sky Survey (SDSS) and Dark Energy Survey (DES) discovered several tens of them (Drlica-Wagner et al. 2015; Newton et al. 2018; Simon et al. 2019), solving the so-called substructure problem when extrapolated to the whole sky.

The low surface brightness of dwarf galaxies could be explained in the primordial black hole (PBH) cold dark matter (CDM) scenario (García-Bellido 2017) due to the loss of stars via close encounters with massive primordial black holes comprising the dark matter haloes of all galaxies. In this scenario, stars in the shallow potential wells of dwarf galaxies are more likely to be slingshotted away due to close encounters with DM black holes, acquiring velocities of hundreds to thousands of km s^{-1} (Clesse & García-Bellido 2017). Such hypervelocity stars (HVS), likely unbound to the Milky Way potential, should travel across the sky and their trajectories should point back to the dwarf spheroidal galaxies (dSph) from which they originate. High-velocity stars are also found in the core of globular clusters (GC: Lützgendorf et al. 2012), which may indicate a population of PBH, and in this case also some of them may acquire a velocity above the escape threshold (Clesse & García-Bellido 2017).

In this article, we develop a Bayesian framework for the detection of such close encounters via the correlation of stellar trajectories in the *Gaia* DR2 catalogue (Gaia Collaboration et al. 2016, 2018a) with the trajectories of dwarf and other nearby galaxies and GC. If massive black holes are indeed responsible for the depletion of stars from dwarf galaxies, it is expected that a few slingshot events must have happened in the last 100 million years inside dwarf galaxies in the Milky Way. In particular, since the probability of events is proportional to the density of the dwarf galaxy, one expects the most massive ones to be the source of HVS. Unfortunately, *Gaia* has limited resolution for distant stars and only those relatively close to the Sun are measured with

★ E-mail: francesco.montanari@uam.es (FM); barado@cab.inta-csic.es (DB); juan.garciabellido@uam.es (JG-B)

© 2019 The Author(s)
Published by Oxford University Press on behalf of the Royal Astronomical Society

Downloaded from https://academic.oup.com/mnras/article/490/4/5647/5625932 by guest on 12 February 2026

sufficient accuracy in 6D phase space (we consider stars up to ∼13 kpc).

Recently, Marchetti et al. (2018a) found that some of the observed HVS were *not* pointing away from the centre of the Milky Way, as was naively expected, but rather towards the disc, as if they had originated in the halo of our galaxy. Furthermore, Hattori et al. (2018) reported one star with an orbit having non-negligible probability of having passed near the Large Magellanic Cloud in the past. This prompted us to explore the possible origin of HVS and whether they could originate in the dSph that orbit around the MW within a radius of several tens of kiloparsecs, which could have been travelling for several tens of millions of years from their sources and could have velocities up to ten times larger than typical stellar velocities in the halo.

We compute the close encounter evidence between HVS and Milky Way GC, dwarf and nearby galaxies by studying the posterior distribution of an impact parameter defined based on phase-space and size information. The evolutionary status of HVS scattering candidates is analysed further based on their Hertzsprung–Russell (HR) diagram to confirm that their expected ages are consistent with having travelled over typically large distances.

In Section 2, we illustrate our *Gaia* DR2 HVS catalogue and the data selection for Milky Way GC and nearby galaxies, discussing the distribution and kinematic properties properties of each selection. In Section 3, we outline our Bayesian methodology to evaluate the scattering evidence between HVS and compact objects in GC or nearby galaxies. In Section 4, we give our results. We conclude in Section 5. In Appendix A, we discuss results based on an alternative stellar selection from the one considered throughout the main article. In Appendix B, we define our Galactocentric reference frame. In Appendix C, we provide references for the selected GC and galaxies, as well as orbit data for Sagittarius dSph and HVS compatible with having crossed its trajectory.

2 DATA

2.1 Hypervelocity stars

Our reference catalogue is *Gaia* DR2 (Gaia Collaboration et al. 2016, 2018a), an all-sky survey consisting of more than 1.3 billion stars. It contains accurate accurate positions (α, δ), proper motions ($\mu_{\alpha*}$, μ_δ), parallax (ω), radial velocity, magnitudes and colours for the bright end for ∼7 million stars. We base our analysis on the selection of 7183 262 stars provided by Marchetti et al. (2018a), established with the following quality cuts (see also the *Gaia* DR2 documentation[1] for more information about variable description):

(i) `astrometric_gof_al` <3;
(ii) `astrometric_excess_noise_sig` ≤2;
(iii) −0.23 ≤ `mean_varpi_factor_al` ≤0.32;
(iv) `visibility_periods_used` >8;
(v) `rv_nb_transits` >5.

We further clean the sample as follows:

(i) selecting heliocentric total velocities in the Galactic rest frame large enough compared with their uncertainties, $v - \sigma_v \gtrsim 500\ \mathrm{km\,s^{-1}}$, to mitigate errors in Galactic absolute velocity;
(ii) removing potentially spurious radial velocities (Boubert et al. 2019).[2]

[1] https://gea.esac.esa.int/archive/documentation/GDR2/

[2] The list of possibly contaminated radial velocities is available as ancillary file to arXiv:1901.10460 [astro-ph.SR].

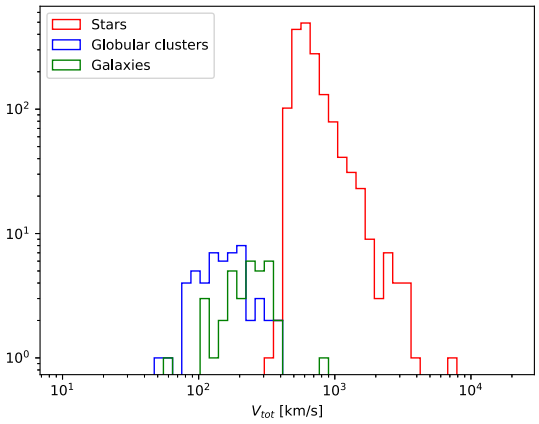


Figure 1. Total velocities in Galactocentric coordinates for our selection of stars, globular clusters and galaxies.

Marchetti et al. (2018a) provides for each star the probability $P_{\rm ub}$ of being unbound from the Milky Way potential. Our final selection of 1649 stars takes into account this information and further photometric and astrometric quality cuts (Schönrich, McMillan & Eyer 2019):

(i) $P_{\rm ub} > 0.5$;
(ii) colour cut $G_{\rm BP} - G_{\rm RP} < 1.5$ mag;
(iii) magnitude cut $G < 14.5$ mag and G, $G_{\rm BP}$, $G_{\rm RP} > 0$ mag;
(iv) BP–RP excess flux factor cut $1.172 < E_{\rm bprp} < 1.3$;
(v) `astrometric_excess_noise` <1.

See Appendix A for an alternative stellar selection.

We consider the distance estimates given in Marchetti et al. (2018a). The catalogue does not include systematic errors in parallax measurements and it sets a large scalelength in the distance prior for likely distant stars that may overestimate distances. To overcome these shortcomings, we also consider the more recent Anders et al. (2019) work, which improves the accuracy of extinction and effective temperature estimates provided with *Gaia* DR2 by combining its astrometric and photometric measurements with external photometric catalogues. In particular, the related distance catalogue includes errors induced by a parallax zero-point offset. We find that Marchetti et al. (2018a) distances are systematically larger on average by roughly a factor of 2 than Anders et al. (2019) estimates for distant stars. The disagreement increases even up to an order of magnitude for stars with distance estimated to be $\lesssim 2$ kpc by Anders et al. (2019), whereas this latter catalogue agrees well with other computations (Bailer-Jones et al. 2018; Schönrich et al. 2019) within this range. Probabilities $P_{\rm ub}$ used for our selection rely on Marchetti et al. (2018a) distances, but evaluating $P_{\rm ub}$ based on Anders et al. (2019) is beyond the scope of the present work. Since $P_{\rm ub}$ does not enter in the following computations, comparing results based on the two different distance estimates still provides a consistency check.

Fig. 1 shows that most of our HVS selection is characterized by total Galactocentric velocities $V_{\rm tot} \sim \mathcal{O}(10^3)\ \mathrm{km\,s^{-1}}$. For details about our coordinate system, see Appendix B. Fig. 2 shows the Toomre diagram with the Galactocentric Cartesian V_y component on the abscissa and the $\sqrt{V_x^2 + V_z^2}$ component on the ordinate.[3] Here and afterwards, error bars indicate 68 per cent confidence

[3] The Toomre diagram is often expressed in terms of Galactic (heliocentric) Cartesian velocities U, V, W (e.g. Schönrich 2012) well suited to describe the

Downloaded from https://academic.oup.com/mnras/article/490/4/5647/5625932 by guest on 12 February 2026

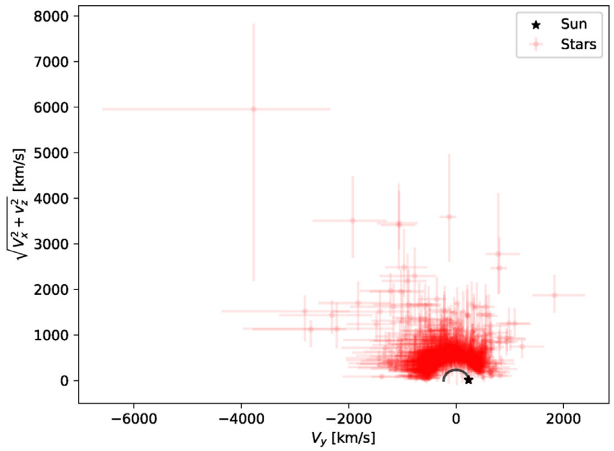


Figure 2. Toomre diagram in terms of Galactocentric Cartesian velocities for our HVS selection. All HVS are above the black semi-circle centred at the origin and of radius given by the Sun's (black star) V_y component.

intervals. The diagram is populated only above a semi-circle centred at the origin, of radius given by the Sun's V_y component, suggesting that we select a population of halo stars (e.g. Bonaca et al. 2017). Fig. 3 shows Galactocentric positions, with error bars dominated by uncertainties in distances from the Sun.

2.2 Globular clusters and galaxies

We select 52 globular clusters (GC) identified in the *Gaia* DR2 catalogue (Gaia Collaboration et al. 2018b) that report both full phase-space and radius, defined as the maximum radius at which proper-motion members are found.

We select all galaxies for which we can match position and half-light radius (measured along major axes), given by McConnachie (2012),[4] with peculiar motions of identified dwarf Milky Way satellite galaxies in *Gaia* DR2 (Fritz et al. 2018). We also include Antlia II (Torrealba et al. 2019) and Andromeda (velocity from van der Marel et al. 2012).[5] In the latter case, we retrieve the optical major axis from the SIMBAD database (Wenger et al. 2000), also used to obtain the sizes and velocities of the Large (LMC) and Small (SMC) Magellanic Clouds, which we combine with the positions listed in McConnachie (2012). This gives a total of 35 galaxies.

Fig. 1 shows total Galactocentric velocities $V_{\rm tot} \sim \mathcal{O}(10^2)\,{\rm km\,s^{-1}}$ for both GC and galaxies. Figs 3 and 4 show GC and galaxy positions, respectively. We verified that the asymmetric GC distribution, concentrated between the Sun and the Galactic Centre, is also present in the full catalogue and not only in our selection (note the lack of GC in the upper quadrants for objects with $x < x_\odot \approx -8.3$ kpc). Fig. 5 shows heliocentric distances and sizes in terms of the radii defined above. GC are characterized by sizes

solar neighborhood. Here we are interested in the dynamics of the Galaxy on a global scale and a Galactocentric frame is more convenient.

[4]We use the table updated on 2015 September 20, available at http://www.astro.uvic.ca/ alan/Nearby_Dwarf_Database.html.

[5]van der Marel et al. (2012) assume $V_y = 239 \pm 5\ {\rm km\,s^{-1}}$ for the Sun Galactocentric velocity component along the direction of Galactic rotation, while here we assume 232.24 ${\rm km\,s^{-1}}$ (see Appendix B). The difference is negligible for our purposes.

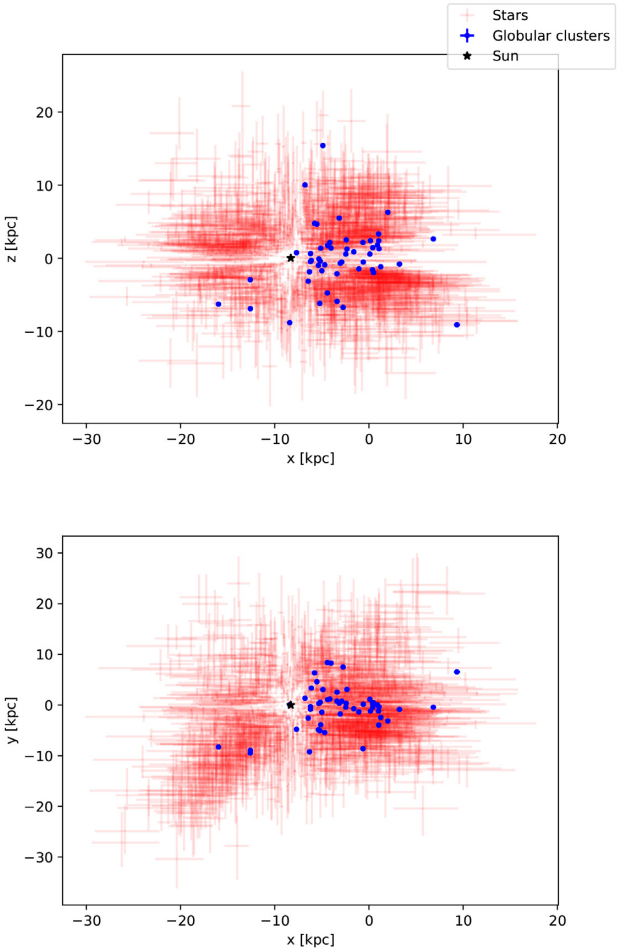


Figure 3. Galactocentric positions for stars and globular clusters. Error bars $\lesssim 3$ per cent for GC are smaller than the markers (the latter are not representative of object extension).

$\mathcal{O}(10)$–$\mathcal{O}(100)$ pc, while galaxies show a larger variation, because we include objects of different types, ranging from dwarfs with radius $\sim \mathcal{O}(10)$ pc to large galaxies such as Andromeda with major semi-axis ~23 kpc. Most galaxies reach distances further than our HVS selection.

Further details about the selected objects are given in Appendix C.

3 METHODOLOGY

3.1 Trajectories

Orbits are integrated using the `gala` software library (Price-Whelan 2017).[6] We use its default Milky Way potential model based on four components. Below, G indicates the gravitational constant, $r_{\rm s}$ is the radial distance in Galactocentric spherical coordinates and $r_{\rm c}$ and $z_{\rm c}$ are the radial distance and height, respectively, in Galactocentric cylindrical coordinates. The nucleus and bulge follow a Hernquist potential for a spheroid (Hernquist 1990):

$$\phi(r_{\rm s}) = -\frac{Gm}{r_{\rm s}+a}\ . \tag{1}$$

[6]https://gala-astro.readthedocs.io

Downloaded from https://academic.oup.com/mnras/article/490/4/5647/5625932 by guest on 12 February 2026

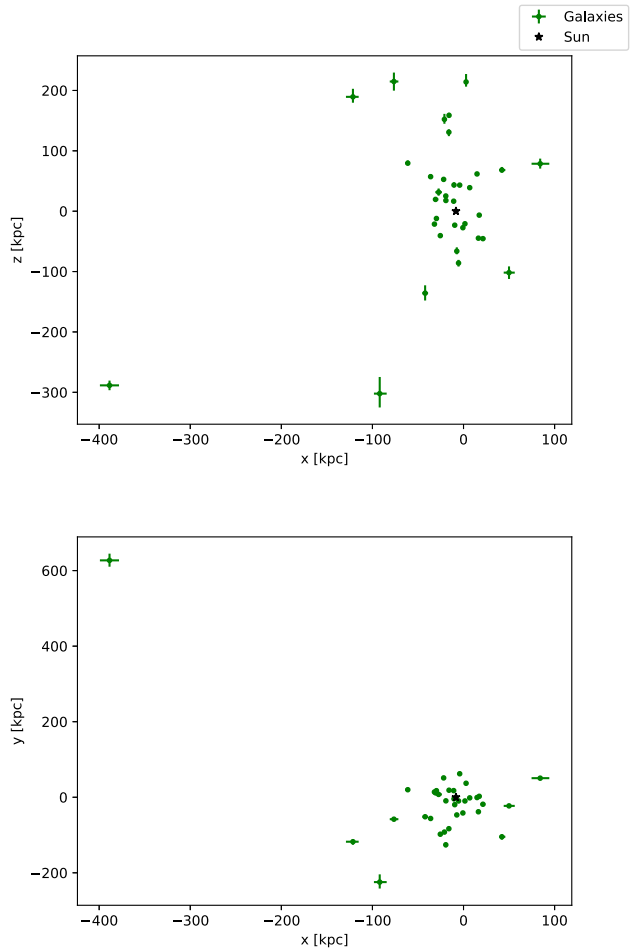


Figure 4. Galactocentric positions for galaxies. The further galaxy is Andromeda. Marker size (for some object larger than error bars) is not representative of object extension.

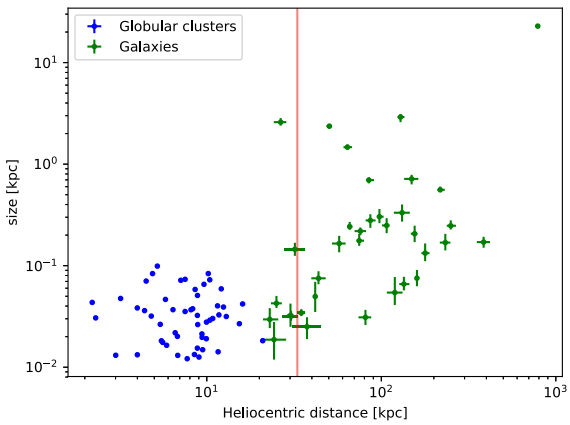


Figure 5. Heliocentric distance and size for GC and galaxies. The vertical line corresponds to the further HVS; the largest object within this distance is Sagittarius dSph, placed at coordinates $(26 \pm 2, 2.6 \pm 0.2)$ kpc.

Table 1. Milky Way potential parameters.

Component	Potential	Parameters
Nucleus	Hernquist	$m = 1.71 \times 10^9\ \mathrm{M}_\odot$ $a = 0.07$ kpc
Bulge	Hernquist	$m = 5 \times 10^9\ \mathrm{M}_\odot$ $a = 1.0$ kpc
Disk	Miyamoto–Nagai	$m = 6.8 \times 10^{10}\ \mathrm{M}_\odot$ $a = 3$ kpc $b = 0.28$ kpc
Halo	NFW	$m = 5.4 \times 10^{11}\ \mathrm{M}_\odot$ $a = 15.62$ kpc

The disc follows a Miyamoto–Nagai profile (Miyamoto & Nagai 1975; Bovy 2015):

$$\phi(r_c, z_c) = -\frac{Gm}{\sqrt{r_c^2 + \left(a + \sqrt{z_c^2 + b^2}\right)^2}} \,. \tag{2}$$

The halo follows a spherical Navarro–Frenk–White (NFW) profile (Navarro, Frenk & White 1996):

$$\phi(r_s) = -\frac{Gm}{r_s} \ln\left(1 + \frac{r_s}{a}\right) \,. \tag{3}$$

We use the same parameters as in Marchetti et al. (2018a), summarized in Table 1. In the PBH CDM scenario, the inner part of the halo is better described by an Einasto profile (Einasto 1965), but this only affects the dynamics close to the Galactic Centre, where a few of our HVS candidates lie. We have verified that taking into account a power-law gravitational potential profile (Evans 1993, 1994; Calcino, Garcia-Bellido & Davis 2018) rather than NFW does not affect our conclusions.

We trace trajectories back in time by 100 Myr and 1 Gyr when looking for correlations between HVS and GC or galaxies, respectively, with a resolution of 1 kyr (necessary to resolve the smallest GC). In the case of large and distant objects (Andromeda, LMC and SMC), we use a poorer time resolution of 100 kyr, but integrate up to 5 Gyr back in time (to assure that the slower stars in our selection have time to reach the Andromeda distance).[7]

3.2 Impact parameter

Let $r(t_i)$ be the distance between a star and a GC or galaxy with radius R (defined as discussed in Section 2) at a given time t_i. We define the impact parameter for the trajectories of a star and a GC/galaxy as

$$\theta \equiv \frac{1}{R} \min_i r(t_i) \,. \tag{4}$$

Given the impact-parameter likelihood $P(D|\theta)$, where D denotes data, we want to identify those stars compatible with having scattered with compact objects bounded to a given GC or galaxy. In the case of GC, the radius is determined via proper motion members and we set $\theta \lesssim 1$ as the necessary condition for scattering. In the case of galaxies, the half-light radius (measured along the major axis) or the optical major semi-axis are looser proxies of the underlying DM distribution. Furthermore, dwarf galaxies can have large ellipticity. We take into account these uncertainties by extending the relevant

[7]More precisely, we integrate orbits setting time steps of 0.1 Myr (10 Myr for Andromeda, LMC and SMC) in `gala` and then interpolate with cubic splines to reach the desired time resolution.

Downloaded from https://academic.oup.com/mnras/article/490/4/5647/5625932 by guest on 12 February 2026

range to $\theta \lesssim 10$ for a star compatible with having scattered with the compact objects bound to a given galaxy, and by studying the results as functions of the impact parameter.

3.3 Likelihoods

We illustrate how we sample from trajectory parameter space based on observables or derived quantities available in the catalogues described in Section 2. Since position errors are dominated by uncertainties in distances, we neglect errors in right ascension α and declination δ for computational convenience.

We write the probability distribution for the star trajectory parameters in terms of log-normal[8] and normal $\mathcal{N}(\mu, \sigma^2)$ distributions:[9]

$$P_* = \text{lognormal}\,(m_d, v_d)\,\mathcal{N}(\boldsymbol{\mu}_{\alpha\beta}, \boldsymbol{\Sigma}_{\mu_{\alpha\beta}})\mathcal{N}(V_r, \sigma^2_{V_r})\,. \tag{5}$$

Here, d is the heliocentric distance discussed in Section 2.1 (we find that a log-normal distribution for distances recovers the respective asymmetric probability distributions), $\boldsymbol{\mu}_{\alpha\beta} = (\mu_{\alpha^*}, \mu_\delta)$ with $\boldsymbol{\Sigma}_{\mu_{\alpha\beta}}$ the covariance matrix ($\mu_{\alpha^*} = \mu_\alpha cos(\delta)$ is proportional to the proper motion in right-ascension direction μ_α, μ_δ is the proper motion in the declination direction) and V_r is the radial velocity. *Gaia* DR2 provides astrometric parameters at epoch J2015.5 that, for comparison with other datasets, we transform to epoch J2000.0 following the reduction procedures used to construct the *Hipparcos* and Tycho catalogues (ESA 1997)[10] (more rigorous transformations, including the effects of light-travel time, are given in Butkevich & Lindegren (2014), but they are not well suited for the negative parallaxes characterizing some of our sources). We verified that the only quantities affected non-negligibly by epoch propagation are α, δ and, for a few sources, V_r.

We write the probability distribution for globular clusters as

$$P_{\rm gc} = \mathcal{N}\,(\boldsymbol{X}, \boldsymbol{\Sigma}_X)\mathcal{N}(\boldsymbol{\mu}_{\alpha\beta}, \boldsymbol{\Sigma}_{\mu_{\alpha\beta}})\mathcal{N}(V_r, \sigma^2_{V_r})\,, \tag{6}$$

where $\boldsymbol{X}$ are heliocentric Cartesian coordinates used to compute distances. In the case of galaxies, we have

$$P_{\rm gal} = \mathcal{N}\left(\mu, \sigma^2_\mu\right)\mathcal{N}(\boldsymbol{\mu}_{\alpha\beta}, \boldsymbol{\Sigma}_{\mu_{\alpha\beta}})\mathcal{N}(V_r, \sigma^2_{V_r}) \times \text{lognormal}(m_R, v_R)\,. \tag{7}$$

Here, the heliocentric distance is computed from the distance modulus μ (for Antlia II, we use the derived distance obtained in Torrealba et al. 2019). For Andromeda, we sample directly from the derived Galactocentric velocity error distributions (van der Marel et al. 2012) rather than proper motions and radial velocity. The log-normal distribution for the radius R takes into account the asymmetric error bounds for some of the objects and the fact that its expectation value is restricted to be positive (we verified that results do not change if we assume a normal distribution and a prior $R > 0$). In the cases of Andromeda, LMC, SMC and GC, we do not have information about the respective radius probability distributions, but this is not critical information, since afterwards we study the results as a function of the impact parameter $\theta \propto 1/R$.

The impact-parameter likelihood $P(D|\theta)$ for every star and GC or galaxy pair is obtained by sampling from $P_* P_{\rm gc}$ or $P_* P_{\rm gal}$, respectively. We reconstruct each likelihood by drawing at least 1000 random samples, necessary to recover Bayes factors at the $\mathcal{O}$(1 per cent) level.[11] We verified that uncertainties in the Galactocentric frame definition (see Appendix B) are negligible for our purposes.[12]

We verified that, for our cases of interest ($\theta \lesssim 10$), likelihoods are well fitted by skew log-normal distributions:[13]

$$P(D|\theta) = \frac{1}{(\theta - \lambda_D)\sigma_D\sqrt{2\pi}} \exp\left[-\frac{(\ln(\theta - \lambda_D) - \mu_D)^2}{2\sigma_D^2}\right]\,, \tag{8}$$

where the fit parameters μ_D, σ_D, λ_D are determined for each star and galaxy/GC pair.

Together with the impact-parameter likelihoods, we also reconstruct the likelihoods for the scattering time (i.e. the time corresponding to the minimum distance between trajectories).

3.4 Hypothesis testing

Given an impact-parameter likelihood and a prior $\Pi(\theta)$, the posterior distribution is given by Bayes' theorem $P(\theta|D) \propto P(D|\theta)\Pi(\theta)$. We can establish at what credible interval a star is compatible with having scattered with compact objects bound to the given system if values $\theta \lesssim \mathcal{O}(1)$ (for GC) or $\theta \lesssim \mathcal{O}(10)$ (galaxies) are included in the region of interest. Below, we consider Bayesian hypothesis testing.

We want to compute the Bayes factor for the hypothesis H that the star trajectory intersects the given galaxy/GC trajectory, relative to the hypothesis $\bar{H}$ of no intersection. Positive evidence for H suggests that the star is compatible with having scattered with compact objects bounded to the given galaxy/GC (possibly fixing a lower threshold for θ).

Given the likelihood $P(D|\theta)$ computed in Section 3.3, the marginal likelihoods under the two hypotheses are

$$P(D|H) = \int_0^\infty \mathrm{d}\theta\; P(D|\theta)\Pi(\theta|H)\,, \tag{9}$$

$$P(D|\bar{H}) = 1 - P(D|H)\,. \tag{10}$$

$\Pi(\theta|H)$ models our prior knowledge on the impact parameter distribution under the trajectories intersection hypothesis. We opt for a flat prior:

$$\Pi(\theta|H) = \begin{cases} \frac{1}{\theta_* - \theta_0}, & \theta_0 \le \theta \le \theta_*, \\ 0, & \text{otherwise.} \end{cases} \tag{11}$$

Finally, the Bayes factor is defined by

$$K(\theta_0, \theta_*) \equiv \frac{P(D|H)}{P(D|\bar{H})}\,. \tag{12}$$

We fix the lower prior threshold θ_0 at the smallest distance from the GC/galaxy centre at which we expect scattering with compact objects. Note that in the PBH CDM scenario, due to the finite size of black holes, the DM density distribution, rather than peaking around a central cusp, may be small in the innermost regions of

[8]The lognormal(m_x, v_x) distribution parameters are related to the mean value x and variance σ_x^2 of the random variable by $m_x = \ln\left(x/\sqrt{1 + \sigma_x^2/x^2}\right)$ and $v_x = \ln\left(1 + \sigma_x^2/x^2\right)$.

[9]Some of the data discussed here provide 16 and 84 per cent quantiles rather than the variance. We approximate the log-normal or normal distribution variance as the mean of these lower and upper bounds.

[10]We use epoch propagation functions provided by TOPCAT (Taylor 2005).

[11]While the sampling can in principle be parallelized over each star and GC/galaxy pair, we are limited by high memory costs to reconstructing only a few likelihoods at the time. This prevents us from running a Markov chain Monte Carlo sampler for each case.

[12]For consistency, we point out that, for the cases shown in the Section 4 figures, we also samplefrom uncertainties in the Galactocentric frame.

[13]While this form is not well suited for $\theta \to 0$, we find it reliable down to our smallest sampled values $\theta \sim \mathcal{O}(10^{-2})$.

Downloaded from https://academic.oup.com/mnras/article/490/4/5647/5625932 by guest on 12 February 2026

the galaxy, due to the gravitational slingshot effect (García-Bellido 2017), and may reach a maximum at a finite distance from the centre. We then study the Bayes factor as a function of the upper threshold θ_*. In other words, we marginalize over the uncertainties outlined in Section 3.2.

Our prior choice is dictated by simplicity, given that here we aim at investigating at once several objects with different mass distributions (in some case highly irregular), dependent not only on the astrophysical details associated with a given object but also on the intrinsic nature of DM. Follow-up analyses focused on individual objects should consider priors based on realistic modelling for ejection location and velocity inside a GC/galaxy. We stress that, the problem being inherently Bayesian (we have at our disposal only one physical realization of the sources under consideration), discussion cannot disregard a prior choice.

Given the flat prior, the marginal likelihood can be written in terms of the likelihood cumulative distribution function (CDF). While we could compute the empirical CDF, it is numerically convenient to use the analytical form obtained by fitting equation (8) and obtain an analytical expression for the marginal likelihood:

$$P(D|H) = \frac{F(\theta_*) - F(\theta_0)}{\theta_* - \theta_0}\,, \tag{13}$$

where $F(x)$ is the CDF up to a given threshold x, given in terms of the CDF for the standard normal distribution Φ:

$$\begin{aligned} F(x) &= \Phi\left(\frac{\ln(x-\lambda_D)-\mu_D}{\sigma_D}\right) \\ &= \frac{1}{2}\left[1+\mathrm{erf}\left(\frac{\ln(x-\lambda_D)-\mu_D}{\sigma_D\sqrt{2}}\right)\right]\,, \end{aligned} \tag{14}$$

where erf is the error function. We verified that differences in Bayes factors computed using the empirical CDF and the analytical approximation are of order 10 per cent for likelihoods peaked in the θ range of interest and within 5 per cent for those objects with $K \gtrsim 1$.

4 RESULTS

We first fix the prior lower threshold $\theta_0 = 0$ and search for scattering events within a given upper threshold θ_*. Then we repeat the search for a few values of the lower prior threshold $\theta_0 \leq 0.5$. This parametrizes our belief that a scattering event is unlikely to take place in the innermost region of a given object, as is the case if we look for interactions with the PBH CDM halo of a galaxy. We consider both Marchetti et al. (2018a) and Anders et al. (2019) distance estimates. If $K > 1$, then the star is compatible with having interacted with a given object.

In the case $\theta_0 = 0$, we do not find candidate scattering events (see, however, Appendix A). As shown in Fig. 6, in the case of the Sagittarius dwarf spheroidal galaxy (Sagittarius dSph), we find two star candidates for having scattered with compact objects within it when assuming Marchetti et al. (2018a) distances for $\theta_0 = 0.36$, corresponding to the minor-to-major axial ratio for Sagittarius dSph, given its ellipticity $\epsilon = 0.64 \pm 0.02$ (McConnachie 2012). The Bayes factor peaks at values $\theta_* \sim 1$. Scattering times are about 20–40 Myr ago, excluding the possibility that these events are directly related to the fact that Sagittarius dSph may have crossed the Galactic disc 300–900 Myr ago (Antoja et al. 2018).

Fig. 7 shows 100 orbits sampled randomly from the respective likelihoods for objects discussed in Fig. 6. Distance uncertainties lead to large spreads in radial direction from the Sun. Trajectories beyond the scattering event are no longer reliable, as they may

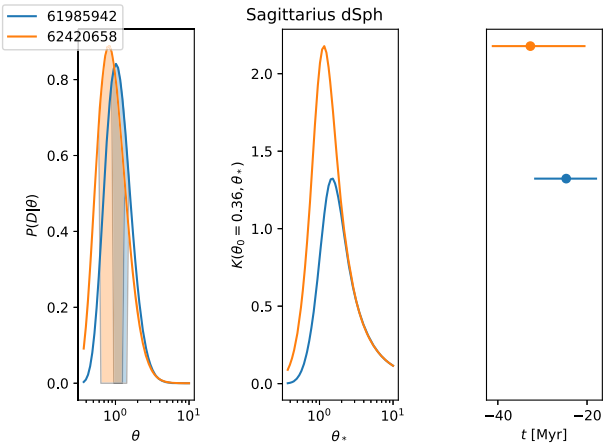


Figure 6. Stars compatible with having scattered with compact objects within Sagittarius dSph, assuming Marchetti et al. (2018a) distances. The legend shows the first eight digits of the *Gaia* DR2 star identification numbers. *Left panel:* impact parameter likelihood. Filled regions are 68 per cent confidence intervals. *Central panel:* Bayes factor for $\theta_0 = 0.36$ as a function of the upper prior threshold θ_*. *Right panel:* mean and 68 per cent intervals for the intersection time (today corresponds to $t = 0$ yr). The height of the error bars is proportional to the respective maximum Bayes factor.

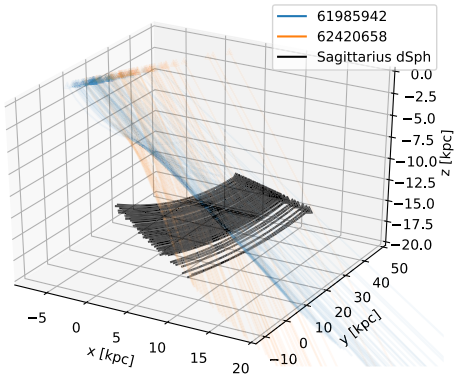


Figure 7. Orbits in Galactocentric Cartesian coordinates corresponding to the same objects discussed in Fig. 6. Line density is proportional to the likelihood. Markers represent positions today.

depend on a different potential, but that is not a concern for our purposes.

In order to verify whether our results are compatible with the evolutionary status of our stars (i.e. whether their lifetime is enough to have crossed the very large distance from the original point), we derive their effective temperature ($T_{\rm eff}$) and bolometric luminosity ($L_{\rm bol}$) and compare these with theoretical isochrones and evolutionary tracks. First, we obtain $L_{\rm bol}$ and $T_{\rm eff}$ using the Virtual Observatory SED Analyzer (VOSA: Bayo et al. 2008), by constructing a complete spectral energy distribution (SED) taking advantage of different photometric repositories under virtual observatory (VO) protocols. Then, the basic properties are derived using atmospheric models by Kurucz (Castelli, Gratton & Kurucz 1997). We impose restrictions on the surface gravity ($\log g = 2$) and metallicity ([Fe/H] $= -0.5$), based on the expectations about these candidates (they should be giant or subgiant stars with low metallicity, since Sagittarius dSph has [Fe/H]$=-0.40 \pm 0.2$ dex: McConnachie 2012). In any case, SED fitting depends weakly on $\log g$ and our results are very similar if a larger degree of freedom is

Downloaded from https://academic.oup.com/mnras/article/490/4/5647/5625932 by guest on 12 February 2026

allowed. Thus, $T_{\rm eff}$ ranges between 6000 and 4250 K, whereas $L_{\rm bol}$ is bracketed between 620 and 2000 $L_{\odot}$. We have compared these values with PADOVA models (Marigo et al. 2017). Their position in a HR diagram clearly shows that they have masses in the range 3.5–6 $M_{\odot}$ and they are either in the subgiant branch, close to the subgiant branch or in the blue loop. Therefore, we can establish a lower limit for the age, about 100 Myr, fully compatible with our expectations.

Positive evidence is not confirmed when using Anders et al. (2019) distances. However, our result provides motivation to model a prior based on the actual three-dimensional DM distribution of Sagittarius dSph, a difficult issue that has to take into account strong tidal disruption.

More information about the sources discussed here is given in Table C4.

5 CONCLUSIONS

We have defined a Bayesian framework to search for correlations between 1642 *Gaia* DR2 high-velocity star trajectories and those of 52 globular clusters (identified by *Gaia* DR2) and 35 Milky Way dwarf and nearby galaxies. We report two star candidates scattered with compact objects within Sagittarius dSph roughly between 20 and 40 Myr ago when assuming the distances estimated in Marchetti et al. (2018a). Analysis of their evolutionary status leads to a lower bound of about 100 Myr for their age, fully compatible with the scattering time window. Results are not confirmed when assuming the distances estimated in Anders et al. (2019).

These events may correspond to DM scattering, if the latter is composed of PBH able to accelerate a star significantly upon encounter. In principle, the reported number of scattering events may be used to validate this hypothesis. However, given the statistically small sample considered here and uncertainties in the PBH mass distribution, we cannot put meaningful limits.

Marchetti et al. (2018a) reported HVS candidates compatible with an extragalactic origin. Their trajectory may also be explained if they scattered with DM bounded to a galaxy or GC. We repeated our search including their final HVS selection of 20 stars (with probability of being unbound larger than 80 per cent) and we do not find evidence to support this hypothesis (furthermore, several stars in their selection are contaminated by spurious radial velocities: Boubert et al. 2019).

In defining the impact parameter based on the radius of a sphere centred around a given galaxy or GC, we have taken into account the necessity of analysing several heterogeneous objects at once. Studying the Bayes factor as a function of the marginal likelihood prior takes into account that the radius is only a proxy of the actual shape (e.g. Sagittarius dSph is characterized by a large ellipticity) or DM distribution (which can extend well beyond the optical size). Nevertheless, a follow-up analysis focused on Sagittarius dSph should define the impact parameter based on its actual shape and DM distribution, taking into account its time evolution.

Our results are highly dependent on the distance computation methodology. We find that Marchetti et al. (2018a) distances are usually significantly larger than those of other catalogues for our stellar selection (see Table C4). Distances estimated in Anders et al. (2019) are more in agreement with other computations (e.g. Bailer-Jones et al. 2018; Schönrich et al. 2019), although results generally differ significantly for stars more distant than 3 kpc. This sensitivity on systematic effects (especially a global parallax zero-point difficult to model) calls for future confirmations based on more accurate parallax estimates.

Marchetti et al. (2018b) showed that the majority of HVS expected to be detected by *Gaia* are fainter than the limiting magnitude required to obtain radial velocities in DR2. Future data releases will include a larger number of stars with full phase-space information, together with improved astronomy and photometry. As our analysis shows, an understanding of systematic errors up to distances of around 10 kpc is crucial for a robust search. More accurate data will also help to avoid spurious HVS identification, which possibly affects our selection.

The fact that we only find candidate scattering events within Sagittarius dSph, relatively large and close, may be due to a selection effect that can be included in future analyses. In fact, if the events under consideration correspond to DM scattering, then we would expect also to be able to detect a similar number of interactions with other large galaxies such as LMC. It is important to repeat and possibly extend the search when future *Gaia* data releases become available.

The main motivation of the present search is that HVS may be correlated to past scattering events with massive compact objects in dwarf galaxies. The same idea prompts another interesting prospect, i.e. using trajectories of HVS compatible with having an extragalactic origin as a guide for the discovery of faint dwarf galaxies, particularly relevant to extending catalogues of low surface brightness galaxies (Du et al. 2019) and for missions like the MESSIER surveyor (Valls-Gabaud & MESSIER Collaboration 2017).

ACKNOWLEDGEMENTS

We thank Alex Drlica-Wagner and Edward (Rocky) Kolb for discussions.

We acknowledge use of the Hydra cluster at IFT-UAM/CSIC (Madrid). This research made use of Astropy,[14] a community-developed core Python package for astronomy (Astropy Collaboration et al. 2013, 2018), TOPCAT (Taylor 2005) and STILTS (Taylor 2006). This work has made use of data from the European Space Agency (ESA) mission *Gaia* (https://www.cosmos.esa.int/gaia), processed by the *Gaia* Data Processing and Analysis Consortium (DPAC, https://www.cosmos.esa.int/web/gaia/dpac/consortium). Funding for the DPAC has been provided by national institutions, in particular the institutions participating in the *Gaia* Multilateral Agreement.

FM and JGB are supported by the Research Project FPA2015-68048-C3-3-P [MINECO-FEDER] and the Centro de Excelencia Severo Ochoa Program SEV-2016-0597. DB is been funded by the Spanish State Research Agency (AEI) Project No. ESP2017-87676-C5-1-R and No. MDM-2017-0737 Unidad de Excelencia 'María de Maeztu' – Centro de Astrobiología (INTA-CSIC).

REFERENCES

Adén D. et al., 2009, A&A, 506, 1147
Anders F. et al., 2019, A&A, 628, A94
Antoja T. et al., 2018, Nature, 561, 360
Astropy Collaboration et al., 2013, A&A, 558, A33
Astropy Collaboration et al., 2018, AJ, 156, 123
Bailer-Jones C. A. L., Rybizki J., Fouesneau M., Mantelet G., Andrae R., 2018, AJ, 156, 58
Bayo A., Rodrigo C., Barrado Y Navascués D., Solano E., Gutiérrez R., Morales-Calderón M., Allard F., 2008, A&A, 492, 277

[14] http://www.astropy.org

Downloaded from https://academic.oup.com/mnras/article/490/4/5647/5625932 by guest on 12 February 2026

Bechtol K. et al., 2015, ApJ, 807, 50
Bellazzini M., Gennari N., Ferraro F. R., Sollima A., 2004, MNRAS, 354, 708
Bellazzini M., Gennari N., Ferraro F. R., 2005, MNRAS, 360, 185
Belokurov V. et al., 2007, ApJ, 654, 897
Belokurov V. et al., 2009, MNRAS, 397, 1748
Blaauw A., 1960, MNRAS, 121, 164
Bonaca A., Conroy C., Wetzel A., Hopkins P. F., Kereš D., 2017, ApJ, 845, 101
Bonanos A. Z., Stanek K. Z., Szentgyorgyi A. H., Sasselov D. D., Bakos G. Á., 2004, AJ, 127, 861
Boubert D. et al., 2019, MNRAS, 486, 2618
Bovy J., 2015, ApJS, 216, 29
Butkevich A. G., Lindegren L., 2014, A&A, 570, A62
Calcino J., Garcia-Bellido J., Davis T. M., 2018, MNRAS, 479, 2889
Carignan C., Beaulieu S., Côté S., Demers S., Mateo M., 1998, AJ, 116, 1690
Carrera R., Aparicio A., Martínez-Delgado D., Alonso-García J., 2002, AJ, 123, 3199
Castelli F., Gratton R. G., Kurucz R. L., 1997, A&A, 318, 841
Chen B. et al., 2001, ApJ, 553, 184
Chou M.-Y. et al., 2007, ApJ, 670, 346
Clesse S., García-Bellido J., 2017, Phys. Dark Univ., 15, 142
Coleman M. G. et al., 2007, ApJ, 668, L43
Dall'Ora M. et al., 2006, ApJ, 653, L109
de Jong J. T. A., Martin N. F., Rix H.-W., Smith K. W., Jin S., Macciò A. V., 2010, ApJ, 710, 1664
Drlica-Wagner A. et al., 2015, ApJ, 813, 109
Du W., Cheng C., Wu H., Zhu M., Wang Y., 2019, MNRAS, 483, 1754
Einasto J., 1965, Trudy Astrofizicheskogo Instituta Alma-Ata, 5, 87
ESA, ed., 1997, The HIPPARCOS and TYCHO catalogues. Astrometric and photometric star catalogues derived from the ESA HIPPARCOS Space Astrometry Mission, ESA Special Publication. Vol. 1200, ESA Publications Division, Noordwijk, the Netherlands
Evans N. W., 1993, MNRAS, 260, 191
Evans N. W., 1994, MNRAS, 267, 333
Fritz T. K., Battaglia G., Pawlowski M. S., Kallivayalil N., van der Marel R., Sohn S. T., Brook C., Besla G., 2018, A&A, 619, A103
Gaia Collaboration et al., 2016, A&A, 595, A1
Gaia Collaboration et al., 2018a, A&A, 616, A1
Gaia Collaboration et al., 2018b, A&A, 616, A12
García-Bellido J., 2017, J. Phys. Conf. Ser., 840, 012032
Gillessen S., Eisenhauer F., Trippe S., Alexand er T., Genzel R., Martins F., Ott T., 2009, ApJ, 692, 1075
Grcevich J., Putman M. E., 2009, ApJ, 696, 385
Greco C. et al., 2008, ApJ, 675, L73
Hattori K., Valluri M., Bell E. F., Roederer I. U., 2018, ApJ, 866, 121
Hernquist L., 1990, ApJ, 356, 359
Ibata R. A., Gilmore G., Irwin M. J., 1994, Nature, 370, 194
Ibata R. A., Wyse R. F. G., Gilmore G., Irwin M. J., Suntzeff N. B., 1997, AJ, 113, 634
Irwin M., Hatzidimitriou D., 1995, MNRAS, 277, 1354
Kirby E. N., Simon J. D., Geha M., Guhathakurta P., Frebel A., 2008, ApJ, 685, L43
Kirby E. N., Guhathakurta P., Bolte M., Sneden C., Geha M. C., 2009, ApJ, 705, 328
Kirby E. N., Lanfranchi G. A., Simon J. D., Cohen J. G., Guhathakurta P., 2011, ApJ, 727, 78
Kirby E. N., Boylan-Kolchin M., Cohen J. G., Geha M., Bullock J. S., Kaplinghat M., 2013, ApJ, 770, 16
Kirby E. N., Simon J. D., Cohen J. G., 2015, ApJ, 810, 56
Koch A., Grebel E. K., Wyse R. F. G., Kleyna J. T., Wilkinson M. I., Harbeck D. R., Gilmore G. F., Evans N. W., 2006, AJ, 131, 895
Koch A. et al., 2009, ApJ, 690, 453
Koposov S. E. et al., 2011, ApJ, 736, 146
Koposov S. E., Belokurov V., Torrealba G., Evans N. W., 2015, ApJ, 805, 130
Laevens B. P. M. et al., 2015a, ApJ, 802, L18
Laevens B. P. M. et al., 2015b, ApJ, 813, 44
Lee M. G., Yuk I.-S., Park H. S., Harris J., Zaritsky D., 2009, ApJ, 703, 692
Lützgendorf N. et al., 2012, A&A, 543, A82
Majewski S. R., Skrutskie M. F., Weinberg M. D., Ostheimer J. C., 2003, ApJ, 599, 1082
Marchetti T., Rossi E. M., Brown A. G. A., 2018a, MNRAS, 490, 157
Marchetti T., Contigiani O., Rossi E. M., Albert J. G., Brown A. G. A., Sesana A., 2018b, MNRAS, 476, 4697
Marigo P. et al., 2017, ApJ, 835, 77
Martin N. F., Ibata R. A., Chapman S. C., Irwin M., Lewis G. F., 2007, MNRAS, 380, 281
Martin N. F. et al., 2008a, ApJ, 672, L13
Martin N. F., de Jong J. T. A., Rix H.-W., 2008b, ApJ, 684, 1075
Martin N. F. et al., 2015, ApJ, 804, L5
Mateo M., Olszewski E. W., Morrison H. L., 1998, ApJ, 508, L55
Mateo M., Olszewski E. W., Walker M. G., 2008, ApJ, 675, 201
McConnachie A. W., 2012, AJ, 144, 4
Miyamoto M., Nagai R., 1975, PASJ, 27, 533
Monaco L., Bellazzini M., Ferraro F. R., Pancino E., 2004, MNRAS, 353, 874
Moretti M. I. et al., 2009, ApJ, 699, L125
Navarro J. F., Frenk C. S., White S. D. M., 1996, ApJ, 462, 563
Newton O., Cautun M., Jenkins A., Frenk C. S., Helly J., 2018, MNRAS, 479, 2853
Norris J. E., Wyse R. F. G., Gilmore G., Yong D., Frebel A., Wilkinson M. I., Belokurov V., Zucker D. B., 2010, ApJ, 723, 1632
Okamoto S., Arimoto N., Yamada Y., Onodera M., 2008, A&A, 487, 103
Peñarrubia J. et al., 2011, ApJ, 727, L2
Pietrzyński G. et al., 2008, AJ, 135, 1993
Pietrzyński G., Górski M., Gieren W., Ivanov V. D., Bresolin F., Kudritzki R.-P., 2009, AJ, 138, 459
Price-Whelan A. M., 2017, The Journal of Open Source Software, 2, 388
Reid M. J., Brunthaler A., 2004, ApJ, 616, 872
Schönrich R., 2012, MNRAS, 427, 274
Schönrich R., Binney J., Dehnen W., 2010, MNRAS, 403, 1829
Schönrich R., McMillan P., Eyer L., 2019, MNRAS, 487, 3568
Simon J. D., Geha M., 2007, ApJ, 670, 313
Simon J. D. et al., 2011, ApJ, 733, 46
Simon J. D. et al., 2019, BAAS, 51, 409
Taylor M. B., 2005, in Shopbell P., Britton M., Ebert R., eds, ASP Conf. Ser. Vol. 347, Astronomical Data Analysis Software and Systems XIV. Astron. Soc. Pac., San Francisco, p. 29
Taylor M. B., 2006, in Gabriel C., Arviset C., Ponz D., Enrique S., eds, ASP Conf. Ser. Vol. 351, Astronomical Data Analysis Software and Systems XV. Astron. Soc. Pac., San Francisco, p. 666
Torrealba G. et al., 2019, MNRAS, 488, 2743
Valls-Gabaud D., 2016, in Proceedings of the International Astronomical Union. Vol. 11, Cambridge University Press, Cambridge UK, p. 199
van der Marel R. P., Fardal M., Besla G., Beaton R. L., Sohn S. T., Anderson J., Brown T., Guhathakurta P., 2012, ApJ, 753, 8
Walker M. G., Mateo M., Olszewski E. W., Gnedin O. Y., Wang X., Sen B., Woodroofe M., 2007, ApJ, 667, L53
Walker M. G., Mateo M., Olszewski E. W., 2008, ApJ, 688, L75
Walker M. G., Mateo M., Olszewski E. W., 2009a, AJ, 137, 3100
Walker M. G., Belokurov V., Evans N. W., Irwin M. J., Mateo M., Olszewski E. W., Gilmore G., 2009b, ApJ, 694, L144
Walker M. G., Mateo M., Olszewski E. W., Peñarrubia J., Evans N. W., Gilmore G., 2009c, ApJ, 704, 1274
Walsh S. M., Willman B., Sand D., Harris J., Seth A., Zaritsky D., Jerjen H., 2008, ApJ, 688, 245
Wenger M. et al., 2000, A&AS, 143, 9
Wilkinson M. I., Kleyna J. T., Evans N. W., Gilmore G. F., Irwin M. J., Grebel E. K., 2004, ApJ, 611, L21
Willman B. et al., 2006, preprint (arXiv:astro-ph/0603486)
Willman B., Geha M., Strader J., Strigari L. E., Simon J. D., Kirby E., Ho N., Warres A., 2011, AJ, 142, 128
Zucker D. B. et al., 2006, ApJ, 650, L41

Downloaded from https://academic.oup.com/mnras/article/490/4/5647/5625932 by guest on 12 February 2026

APPENDIX A: ALTERNATIVE STELLAR SELECTION

As an alternative to the stellar selection mentioned in Section 2.1, here we consider 1747 stars that still satisfy cuts given in Marchetti et al. (2018a), have total heliocentric velocities $v - \sigma_v \gtrsim 500\,\mathrm{km\,s^{-1}}$ and exclude possibly contaminated radial velocities (Boubert et al. 2019), but have a higher unbound probability threshold $P_{\rm ub} > 0.9$. Most of the stars have negative parallax, an indicator of poor data quality due to the absence of further photometric and astrometric cuts.

Assuming Marchetti et al. (2018a) distances and setting a lower prior threshold $\theta_0 = 0$ for the computation of the Bayes factor, the same search described in Section 4 yields Fig. A1. Two stars are compatible with having scattered with compact objects in Sagitarius dSph 10–30 Myr ago. If we set $\theta_0 = 0.36$, as discussed in Section 4, we find that the maximum Bayes factors increases to $K \sim 2$, 10 for stars 52292628 and 62557247, respectively, and that a third star (62779130) has positive scattering evidence ($K \gtrsim 1$). We verified that all stars are compatible with being at least ∼80 Myr old. (More information about these sources is given in Table C4.)

However, results are not confirmed when we repeat the same search assuming Anders et al. (2019) distances. Furthermore, Anders et al. (2019) flag the aforementioned stars as possible spurious astrometry, due to the large renormalized unit-weight error (RUWE). Hence, in this case positive evidence for scattering events may be driven not only by distance estimate systematic errors but also by a poor astrometric fit.

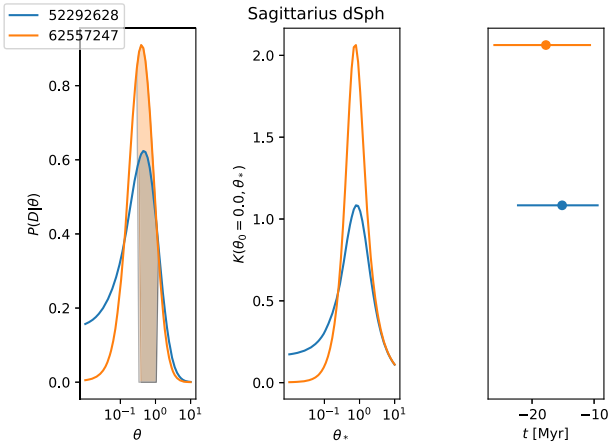


Figure A1. Same as Fig. 6, but for different stars. The Bayes factor in the central panel is computed by setting a lower prior threshold $\theta_0 = 0$.

APPENDIX B: GALACTOCENTRIC COORDINATES

Galactocentric coordinates are defined as a Cartesian right-handed system with the x-axis pointing from the position of the Sun projected on the Galactic midplane to the Galactic Centre, the y-axis pointing roughly towards Galactic longitude $\ell = 90^\circ$ and the z-axis pointing roughly towards the North Galactic Pole (we define the Galactic plane to be the normal to the north pole of Galactic coordinates defined by Blaauw 1960). The Galactic Centre right ascension and declination are taken to be $\alpha = 17{:}45{:}37.224$ hr and $\delta = -28{:}56{:}10.23$ deg, respectively (Reid & Brunthaler 2004). We assume the distance from the Sun to the Galactic Centre to be 8.33 ± 0.35 kpc (Gillessen et al. 2009) and its height above the Galactic midplane to be 27 ± 4 pc (Chen et al. 2001). Galactocentric velocities are definied assuming a circular velocity of 220 $\mathrm{km\,s^{-1}}$ at solar radius (Bovy 2015) and a Sun peculiar velocity with respect to the Galactic Centre $(V_x, V_y, V_z)_\odot = (11.1 \pm 0.74 \pm 1, 12.24 \pm 0.47 \pm 2, 7.25 \pm 0.37 \pm 0.5)$ $\mathrm{km\,s^{-1}}$, with additional systematic errors (1, 2, 0.5) $\mathrm{km\,s^{-1}}$ (Schönrich, Binney & Dehnen 2010).

APPENDIX C: ORBITS DATA

Tables C1 and C2 list source identifiers for GC and galaxies used in the main analysis. Table C3 shows Sagittarius dSph phase-space data and size. Table C4 shows phase-space data and derived quantities for *Gaia* DR2 stars compatible with having scattered with compact objects within Sagittarius dSph when assuming Marchetti et al. (2018a) distances.

GC, galaxy and star catalogues are available as ancillary files at https://arxiv.org/abs/1907.09298.

Table C1. Globular cluster identifiers.

NGC 0104	NGC 5272	NGC 6218	NGC 6388	NGC 6656
NGC 0288	NGC 5286	NGC 6254	NGC 6397	NGC 6681
NGC 0362	NGC 5466	NGC 6266	NGC 6440	NGC 6752
NGC 1851	NGC 5897	NGC 6273	NGC 6453	NGC 6779
NGC 1904	NGC 5904	NGC 6284	NGC 6522	NGC 6809
NGC 2298	NGC 5986	NGC 6287	NGC 6535	NGC 6838
NGC 2808	NGC 6093	NGC 6293	NGC 6541	NGC 6864
NGC 3201	NGC 6121	NGC 6304	NGC 6544	NGC 7078
NGC 4372	NGC 6144	NGC 6341	NGC 6626	NGC 7089
NGC 4833	NGC 6171	NGC 6352	NGC 6637	NGC 7099
NGC 5139	NGC 6205			

Downloaded from https://academic.oup.com/mnras/article/490/4/5647/5625932 by guest on 12 February 2026

Table C2. Nearby galaxy identifiers and detailed references (complementing those given in Section 2.2) for position, size and other useful measurements. All systems are identified as dwarf galaxies, excluding Andromeda, the Large Magellanic Cloud (LMC), Small Magellanic Cloud (SMC) and objects of ambiguous nature denoted by an asterisk (*).

*Draco II	Laevens et al. (2015b)
*Grus 1	Koposov et al. (2015)
*Horologium 1	Koposov et al. (2015), Bechtol et al. (2015)
*Reticulum 2	Bechtol et al. (2015), Koposov et al. (2015)
*Triangulum II	Laevens et al. (2015a)
*Tucana III	Drlica-Wagner et al. (2015)
Andromeda	See Section 2.2
Antlia II	See Section 2.2
Bootes (I)	Dall'Ora et al. (2006), Martin et al. (2007), Martin, de Jong & Rix (2008b), Koposov et al. (2011), Grcevich & Putman (2009), Norris et al. (2010)
Bootes II	Walsh et al. (2008), Koch et al. (2009), Martin et al. (2008b), Grcevich & Putman (2009)
Canes Venatici (I)	Martin et al. (2008a), Simon & Geha (2007), Martin et al. (2008b), Grcevich & Putman (2009), Kirby et al. (2008), Kirby et al. (2011)
Canes Venatici II	Greco et al. (2008), Simon & Geha (2007), Martin et al. (2008b), Grcevich & Putman (2009), Kirby et al. (2008), Kirby et al. (2011)
Carina	Pietrzyński et al. (2009), Walker, Mateo & Olszewski (2009a), Irwin & Hatzidimitriou (1995), Walker, Mateo & Olszewski (2008), Grcevich & Putman (2009), Koch et al. (2006)
Coma Berenices	Belokurov et al. (2007), Simon & Geha (2007), Martin et al. (2008b), Grcevich & Putman (2009), Kirby et al. (2008), Kirby et al. (2011)
Draco	Bonanos et al. (2004), Walker et al. (2007), Martin et al. (2008b), Wilkinson et al. (2004), Grcevich & Putman (2009), Kirby et al. (2011)
Eridanus 2	Koposov et al. (2015), Bechtol et al. (2015)
Fornax	Pietrzyński et al. (2009), Walker et al. (2009a), Irwin & Hatzidimitriou (1995), Walker et al. (2008), Walker et al. (2009b), Grcevich & Putman (2009), Kirby et al. (2011)
Hercules	Coleman et al. (2007), Adén et al. (2009), Martin et al. (2008b), Grcevich & Putman (2009), Kirby et al. (2008), Kirby et al. (2011)
Hydra II	Martin et al. (2015), Kirby, Simon & Cohen (2015)
LMC	See Section 2.2
Leo I	Bellazzini et al. (2004), Mateo, Olszewski & Walker (2008), Irwin & Hatzidimitriou (1995), Grcevich & Putman (2009), Kirby et al. (2011)
Leo II	Bellazzini, Gennari & Ferraro (2005), Walker et al. (2007), Irwin & Hatzidimitriou (1995), Grcevich & Putman (2009), Kirby et al. (2011)
Leo IV	Moretti et al. (2009), Simon & Geha (2007), de Jong et al. (2010), Grcevich & Putman (2009), Kirby et al. (2008), Kirby et al. (2011)
Leo V	
SMC	See Section 2.2
Sagittarius dSph	Ibata, Gilmore & Irwin (1994), Ibata et al. (1997), Mateo, Olszewski & Morrison (1998), Majewski et al. (2003), Monaco et al. (2004), Chou et al. (2007), Grcevich & Putman (2009), Peñarrubia et al. (2011)
Sculptor	Pietrzyński et al. (2008), Walker et al. (2009a), Irwin & Hatzidimitriou (1995), Walker et al. (2008), Carignan et al. (1998), Grcevich & Putman (2009), Kirby et al. (2009), Kirby et al. (2011)
Segue (I)	Belokurov et al. (2007), Simon et al. (2011), Martin et al. (2008b), Grcevich & Putman (2009), Norris et al. (2010)
Segue II	Belokurov et al. (2009), Kirby et al. (2013)
Sextans (I)	Lee et al. (2009), Walker et al. (2009a), Irwin & Hatzidimitriou (1995), Walker et al. (2008), Grcevich & Putman (2009), Kirby et al. (2011)
Tucana 2	Koposov et al. (2015), Bechtol et al. (2015)
Ursa Major (I)	Okamoto et al. (2008), Simon & Geha (2007), Martin et al. (2008b), Grcevich & Putman (2009), Kirby et al. (2008), Kirby et al. (2011)
Ursa Major II	Zucker et al. (2006), Simon & Geha (2007), Martin et al. (2008b), Grcevich & Putman (2009), Kirby et al. (2008), Kirby et al. (2011)
Ursa Minor	Carrera et al. (2002), Walker et al. (2009c), Irwin & Hatzidimitriou (1995), Wilkinson et al. (2004), Grcevich & Putman (2009), Kirby et al. (2011)
Willman 1	Willman et al. (2006), Martin et al. (2007), Martin et al. (2008b), Grcevich & Putman (2009), Willman et al. (2011)

Table C3. Sagittarius dSph phase-space and size data. Rows correspond to right ascension α and declination δ (ICRS at epoch J2000.0), distance modulus μ, proper motions in the right-ascension direction $\mu_{\alpha*} = \mu_\alpha \cos\delta$ and in the declination direction μ_δ, radial velocity along the line of sight V_r and half-light radius measured along the major axis r_h.

α [deg]	283.8313
δ [deg]	−30.4606
μ	17.13 ± 0.11
$\mu_{\alpha*}$ [mas yr^{-1}]	-2.736 ± 0.044
μ_δ [mas yr^{-1}]	-1.357 ± 0.043
V_r [km s^{-1}]	140 ± 2
r_h [arcmin]	342 ± 12

Downloaded from https://academic.oup.com/mnras/article/490/4/5647/5625932 by guest on 12 February 2026

Table C4. HVS compatible with having scattered with compact objects within Sagittarius dSph. Columns correspond to *Gaia* DR2 source identifier, RA and declination, parallax, proper motion in the RA direction $\mu_{\alpha*} = \mu_{\alpha*}\cos(\delta)$, proper motion in the declination direction, proper motion correlation coefficient, radial velocity and heliocentric distance derived in Marchetti et al. (2018a), heliocentric distance derived in Anders et al. (2019) and probability of being unbound from the Milky Way potential. The unbound probability relies on Marchetti et al. (2018a) distances. The reference epoch for astrometric quantities is J2015.5. While here we report the full source identifier, in the main text we only refer to the first eight digits. The first two stars are discussed in Section 4, the others in Appendix A.

Source	(α, δ) [deg]	ϖ [mas]	$\mu_{\alpha*}$ [mas yr^{-1}]	μ_δ [mas yr^{-1}]	$c_{\mu_{\alpha*}\mu_\delta}$	V_r [km s^{-1}]	$d_{\rm Marchetti}$ [kpc]	$d_{\rm Anders}$ [kpc]	$P_{\rm ub}$
6198594250104473728	(223.0436, −37.9298)	0.10 ± 0.04	−21.14 ± 0.06	2.40 ± 0.05	−0.12	96.0 ± 1.3	$9.4^{+3.3}_{-2.0}$	$5.8^{+1.9}_{-1.3}$	0.87
6242065813132837376	(241.4245, −24.0908)	0.08 ± 0.04	−11.97 ± 0.07	2.71 ± 0.04	0.03	−60.5 ± 1.3	$11.7^{+4.8}_{-3.0}$	$7.2^{+1.8}_{-1.8}$	0.54
5229262874909180928	(162.8655, −73.4932)	−3.79 ± 1.14	−30.45 ± 2.16	38.96 ± 2.12	−0.08	51.9 ± 1.3	$8.6^{+4.8}_{-3.2}$	$2.0^{+1.8}_{-0.5}$	0.97
6255724732546338688	(228.2981, −20.7720)	−2.59 ± 0.73	−31.37 ± 1.42	10.88 ± 1.36	−0.12	−109.3 ± 0.8	$8.6^{+5.3}_{-3.6}$	$2.3^{+1.9}_{-0.8}$	0.93
6277913053288720512	(214.1732, −20.3474)	−2.02 ± 0.43	−40.19 ± 0.69	11.60 ± 0.54	−0.22	−39.7 ± 2.9	$10.1^{+5.5}_{-3.3}$	$4.3^{+2.5}_{-1.4}$	1.00

This paper has been typeset from a TEX/LATEX file prepared by the author.

Downloaded from https://academic.oup.com/mnras/article/490/4/5647/5625932 by guest on 12 February 2026